

Partial Oxidation of Methane to Acetic Acid with Oxygen Using AuPd/ZSM-5

Xu Li, Guodong Qi, Richard J. Lewis, Mark J. Howard, Barry A. Murrer, Brian Harrison, David J. Morgan, Christopher J. Kiely, Qian He, Thomas E. Davies, David J. Willock, Michael Bowker, Jingxian Cao, Feng Deng, Jun Xu,* and Graham J. Hutchings*



Cite This: *ACS Catal.* 2025, 15, 18663–18674



Read Online

ACCESS |



Metrics & More



Article Recommendations

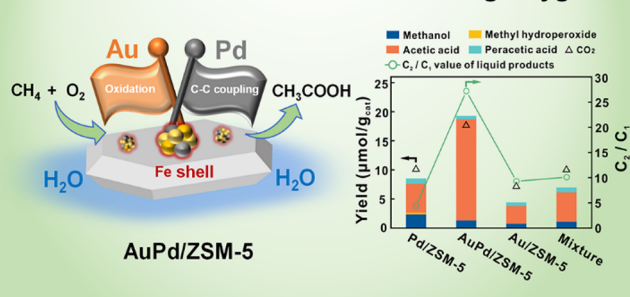


Supporting Information

ABSTRACT: The selective oxidation of methane to form methanol and acetic acid has been studied using AuPd nanoparticles supported on the zeolite H-ZSM-5 in water at 240 °C using molecular oxygen as the terminal oxidant in the absence of any added coreductant. The addition of Pd to Au/ZSM-5 significantly increases the selectivity to acetic acid to levels approaching almost complete selectivity within the oxygenated products. However, we observe that the reaction conditions employed lead to the corrosion of the stainless-steel components of the autoclave reactor and also leaching of iron from the ZSM-5 zeolite, and hence the AuPd nanoparticles, on reaction, become coated or partially coated with an oxidic Fe shell. The presence of the oxidized iron coating hinders nanoparticle agglomeration preventing deactivation of the AuPd/ZSM-5 catalyst but does not adversely affect the observed catalysis.

KEYWORDS: methane oxidation, AuPd nanoparticles, zeolite, acetic acid, heterogeneous catalysis

Methane Oxidation to Acetic Acid using Oxygen



INTRODUCTION

Methane, the primary component of natural gas, shale gas, and biogas, represents Earth's most plentiful carbon resource. Traditionally, this resource has been utilized via direct combustion for heat, electricity, and transportation, leading to significant CO₂ emissions.¹ However, climate change and the push for carbon neutrality necessitate a paradigm shift in methane utilization.² Partial methane oxidation (PMO) to generate valuable oxygenated products has emerged as a highly sought-after catalytic reaction. Compared to alternative methane conversion methods like syngas-mediated methanol synthesis,^{3,4} oxidative coupling of methane (OCM),⁵ and methane dehydrogenation to aromatics (MDA),^{6,7} PMO may offer potential for superior atomic utilization efficiency, lower energy consumption, and reduced CO₂ emissions. The inherent inertness of methane, characterized by its strong C–H bond (435 kJ/mol), can be addressed by the use of harsh reaction conditions or potent oxidants. Illustrative examples include homogeneous PMO reactions catalyzed by Pd⁸ or Hg^{9,10} complexes, as well as Au cations.¹¹ These systems often employ aggressive oxidants, such as sulfur trioxide and highly concentrated sulfuric acid.

Nature provides a captivating example of PMO under mild conditions with the enzymatic methane monooxygenase (MMO) system, which utilizes molecular oxygen to convert methane to methanol.^{12–15} Inspired by this biological process,

researchers are actively pursuing the development of biomimetic solid catalysts for PMO at lower temperatures and with milder oxidants, such as N₂O, O₂, and H₂O₂. Iron-based (Fe) catalysts^{16–18} exhibit high selectivity for methanol when using N₂O as an oxidant, while Cu-zeolite catalysts^{19–21} excel with O₂. The active centers responsible for this activity are believed to be Fe- α -oxygen species and [Cu–O–Cu] clusters, respectively, functioning effectively in gas-phase PMO to methanol even at low temperatures, including room temperature. However, these reactions often necessitate product release through water extraction due to the continued attachment of methanol precursors to the catalyst. In this way, Cu-zeolite catalysts can utilize H₂O as the source of oxygen in PMO products.²² Although initially considered stoichiometric processes, recent breakthroughs have reported closed catalytic cycles for PMO over Cu-zeolites, enabling continuous operation with H₂O and O₂ feeds.^{23,24}

Received: June 7, 2025

Revised: October 18, 2025

Accepted: October 20, 2025

Aqueous PMO offers exciting possibilities with various oxidants and catalysts. Supported Fe or FeCu catalysts using H_2O_2 as the oxidant exhibit high selectivity toward formic acid or acetic acid.^{25–28} Interestingly, studies on Au–Pd catalysts with H_2O_2 and isotopically labeled oxygen ($^{18}\text{O}_2$) revealed that only 30% of the oxygen in methanol product originated from H_2O_2 , suggesting that H_2O_2 activates methane for subsequent oxidation by molecular oxygen.^{29,30} Furthermore, these catalysts can achieve PMO with in situ-generated H_2O_2 from H_2 and O_2 .³¹ For Rh-ZSM-5 zeolites, utilizing O_2 with CO as a coreactant leads to high production of methanol and acetic acid.^{32,33} Notably, these catalysts lack PMO activity solely with O_2 . Recent breakthroughs include catalysts exhibiting PMO activity with O_2 alone. For instance, a hydrogen-reduced Pd-containing phosphomolybdate catalyst achieves nearly 100% selectivity toward methanol under these conditions.³⁴ Additionally, edge-rich MoS_2 catalysts showcase remarkable room-temperature PMO activity to C_1 oxygenates using just O_2 .³⁵ Our recent work explored aqueous PMO with Au nanoparticles supported on the ZSM-5 zeolite (Au-ZSM-5) using only molecular oxygen (O_2) and no coreductant.³⁶ This system gave methanol and acetic acid as primary products within a temperature range of 120–240 °C. While Au nanoparticles served as the active sites, the acid sites in ZSM-5 played a crucial role in stabilizing the active sites and boosting the catalytic performance.³⁷ We proposed parallel pathways for methanol and acetic acid formation involving parallel C_1 oxidation and C–C coupling pathways through a network of surface-mediated processes. Furthermore, incorporating carbon additives significantly enhanced catalytic performance and methanol selectivity. This phenomenon is attributed to surface interactions between oxidized carbon species and the Au-ZSM-5 catalyst.³⁸ This discovery highlights the potential for coreactant oxidation to influence PMO reactions, leading to diverse reaction pathways and performances. Most recently, we found that during the reaction under the aggressive reaction conditions, the Au nanoparticles in the Au/ZSM-5 catalyst become coated with an iron oxide overlayer caused by iron being leached from the autoclave reactor, but this iron oxide overlayer did not have any adverse effects on the observed catalysis.³⁹

In our earlier studies, we have shown that the addition of Pd to Au to form an alloy can greatly enhance the catalytic activity for selective oxidation.⁴⁰ In view of this, we have investigated PMO with AuPd alloy nanoparticles supported on H-ZSM-5 and demonstrate that the addition of Pd to Au significantly enhances the selectivity to acetic acid when methane is reacted with oxygen in water at 240 °C. However, traditional reactor materials for high pressure PMO reactions, such as stainless-steel, are not completely resistant to corrosion under the reaction conditions used. This can lead to leaching of corrosion products, potentially acting as unintended PMO reaction additives. For example, Fe-leaching from reactor components could significantly impact PMO performance, particularly in industrial settings, where using PTFE liners or entirely corrosion-resistant parts might not be practical. However, the influence of reactor corrosion and metal leaching on the PMO has received limited research attention to date.

In this paper, we investigate how Fe species, originating from either the reactor or the ZSM-5 support, influence the catalytic activity of AuPd/ZSM-5 for methane oxidation to acetic acid. We observe a modest increase in oxygenates, mainly acetic acid, when the oxidation was carried out in a stainless-steel reactor compared to a glass-lined reactor. The stainless-steel reactor and

ZSM-5 support are both found to leach Fe species during the reaction, leading to an oxidic Fe species coating the AuPd alloy on the AuPd/ZSM-5 catalyst after the reaction.

EXPERIMENTAL SECTION

Note on Safe Operation of Experiments. When conducting catalytic oxidation, it is important to ensure that reaction conditions are such that the experiments are not conducted in the explosion region. For methane oxidation, Cooper and Wiezevich⁴¹ have shown that experiments conducted with $\leq 14\%$ O_2 even at elevated temperature and pressure are outside the explosive region and this is the case in the work reported here.

Materials and Reagents. H-ZSM-5 zeolites ($\text{SiO}_2/\text{Al}_2\text{O}_3 = 25$) were obtained from Nankai University Catalyst Co. Ltd. Gold chloride trihydrate ($\text{HAuCl}_4 \cdot 3\text{H}_2\text{O}$, $\geq 49.0\%$ Au basis) was purchased from Sigma. Palladium chloride (PdCl_2 , $\geq 59.0\%$ Pd basis), aqueous ammonia (25–28%), iron nitrate nonahydrate ($\text{Fe}(\text{NO}_3)_3 \cdot 9\text{H}_2\text{O}$, 99.8%), iron chloride (FeCl_3 , $\geq 97.0\%$), and iron oxide (Fe_2O_3 , 99.8%, particle size of $< 1 \mu\text{m}$) were obtained from Sinopharm Chemical Reagent Co., Ltd. Fine iron powder (Fe, $\geq 98.0\%$, particle size of $< 38 \mu\text{m}$) was obtained from Aladdin. Methane (99.999%) was obtained from Dalian Special Gases Co., Ltd. Nitrogen (99.999%) and oxygen (99.999%) were obtained from Wuhan Huaxing Industrial Gas Co., Ltd. $^{13}\text{CH}_4$ (^{13}C , 99%, 99.9% chemical purity) was purchased from Cambridge Isotope Laboratories, Inc. The ^{13}CO (^{13}C , 99%) was purchased from Cambridge Isotope Laboratories. All materials and reagents were used directly without purification.

Catalyst Preparation. Prior to metal deposition, the as-received zeolitic material (NH_4 -ZSM-5) was first exposed to an oxidative heat treatment (550 °C at 3 °C/min for 6 h). Typically, 2.0 g of the NH_4 -ZSM-5 zeolite was put in a ceramic boat and calcined under an air atmosphere using a tubular furnace. The temperature was programmed from ambient temperature up to 550 °C with a ramp of 3 °C/min, and after being kept at 550 °C for 6 h, the sample was cooled to ambient temperature naturally.

AuPd/ZSM-5 Catalyst. 0.5 wt % AuPd/ZSM-5 catalysts were prepared by a deposition–precipitation method using aqueous ammonia as the base to control the pH value. This method was used to ensure that the prepared catalysts contained no adventitious carbon impurities. A solution of the Au and Pd metal salts was added to deionized water (66.7 mL) and mixed together by 5 min stirring, then the zeolite (1.0 g) was added, and the mixture was stirred (600 rpm) to a thin slurry. The solution of mixed Au and Pd metal salts was prepared by mixing the required amount of HAuCl_4 aqueous solution ($[\text{Au}] = 6.0 \text{ mmol L}^{-1}$) and PdCl_2 aqueous solution ($[\text{Pd}] = 6.0 \text{ mmol L}^{-1}$) to control the loading of each metal. An appropriate amount of 2.5 wt % aqueous ammonia solution was also slowly added at room temperature over 30 min to the above mixture until the desired pH value was reached (typically pH 10). The resulting mixture was aged (60 °C, 2 h) with stirring at 600 rpm. Then, the sample was filtered and washed thoroughly with deionized water. The sample was dried in an oven (80 °C, 16 h) and calcined in a tubular furnace in static air (room temperature to 240 °C at 3 °C min^{-1} and held at 240 °C for 90 min, and then cooled to room temperature). Au/ZSM-5 and Pd/ZSM-5 monometallic catalysts were prepared in an analogous manner using Au or Pd salt alone. All the samples were prepared at a pH value of 10 and aging time of 2 h unless otherwise stated.

Acid-Treated ZSM-5 Support. H-ZSM-5 (1.0 g) was dispersed in aqueous HCl (5 wt %, 30 mL, Sinopharm Chemical Reagent Co., Ltd.) and stirred at 80 °C for 12 h, then filtered, and thoroughly washed with deionized water until a pH value of 7 for the washing water was reached. After drying (120 °C, 16 h), the sample, denoted as ZSM-5-At, was used to prepare the AuPd/ZSM-5-At catalyst following the same procedure as that described above.

Catalyst Characterization. X-ray Diffraction (XRD). Powder X-ray diffraction (XRD) measurements were recorded on a PANalytical X'Pert Powder X-ray diffraction diffractometer with Cu K α ($\lambda = 1.5406 \text{ \AA}$), with the recording beam voltage at 40 kV, current at 40 mA, and scanning speed of 0.2 °/s.

Inductively Coupled Plasma Optical Emission Spectroscopy (ICP-OES). The Au, Pd, and Fe contents of the fresh and used AuPd/ZSM-5 samples were analyzed using an Agilent ICP-OES 730 inductively coupled plasma optical emission spectrometer.

Spherical Aberration-Corrected Transmission Electron Microscopy (AC-TEM). Initial microscopy was conducted on an aberration-corrected ThermoFisher Scientific Spectra 200 with a Super-X energy-dispersive spectrometer (EDS) operating at 200 kV with a convergence angle of 29.5 mrad and a probe current of 80 pA. Additional high-angle annular dark-field imaging and EDS mapping were performed by using an aberration-corrected JEOL ARM200CF microscope equipped with a cold field-emission gun operating at 200 kV. Samples were prepared by dry dispersion of the catalyst powder over holey carbon-coated 300 mesh copper grids.

X-ray Photoelectron Spectroscopy (XPS). XPS spectra were obtained with a Thermo Fisher Scientific K-alpha⁺ photoelectron spectrometer, using a microfocused monochromatic Al K α radiation source ($h\nu = 1486.6 \text{ eV}$) operating in the 400 μm spot mode, at a power of 72 W (6 mA \times 12 kV). Due to the uncertainty in the C 1s binding energies,⁴² the binding energies, once calibrated to the C 1s peak of adventitious carbon, were checked against the Si 2p peak of the support, which was found to be 103.5 eV. The uncertainty in the binding energies is 0.2 eV. Data was analyzed in CasaXPS and where appropriate was fitted using Voigt-like line shapes derived from bulk materials after removal of a Shirley or linear background and quantified using Scofield sensitivity factors corrected for the electron escape depth according to the TPP-2 M formulation.

Methane Oxidation Reactions. The oxidation reaction of CH₄ with O₂ was conducted in a stainless-steel Parr autoclave reactor, either with or without a quartz glass liner (total volume: 25 mL). Typically, the catalyst (0.1 g), a polytetrafluoroethylene (PTFE)-coated magnetic stirrer, and deionized water (15 mL) were added to the glass liner. The reactor was sealed and purged with pure N₂ for 0.5 h to remove dissolved gases from the suspension. Following this, the reactor was purged three times with methane to eliminate residual N₂. Methane (20.7 bar) and oxygen (3.5 bar) were then introduced into the reactor sequentially with gas partial pressures measured at room temperature. Methane (20.7 bar), oxygen (2.5 bar), and CO (1.0 bar) were used in the CO involved reaction, with the aim to maintain the same total pressure as that without CO.

The mixture was stirred at 1000 rpm for 10 min at room temperature using a magnetic stirrer, ensuring the reaction system reached a stable state. Subsequently, the reactor was heated to the desired reaction temperature of 240 °C within 30 min under 1000 rpm stirring. After maintaining the reaction for 5 to 960 min at 240 °C, the reactor was rapidly cooled in an ice water bath to <10 °C to prevent the loss of liquid products. Gas-

phase products were collected in a gas sampling bag, and liquid-phase products were filtered and collected for liquid NMR analysis. All reactions were conducted three times, and the data presented are the averages of these experiments. The experimental errors are within $\pm 7\%$.

Methane oxidation reactions with the addition of Fe sources were conducted using the same procedure, except that a specified amount of Fe³⁺, Fe powder, or Fe₂O₃ (100, 500, 1000, or 2500 ppm weight (wt.) of the catalyst) was added to the glass liner before sealing the Parr reactor.

Isotopic Tracer Experiments. To trace the fate of the carbon atom from methane and to distinguish its fate from that of the added carbon monoxide, ¹³C-labeled CH₄ (20% in the 20.7 bar) and CO (20% in the 1.0 bar) were used in the reaction with oxygen. A high-sensitivity NMR CryoProbe on a Bruker Avance-600 liquid NMR spectrometer was employed to analyze the liquid products obtained from the isotopic tracing experiments. ¹H NMR spectra were recorded by using a water suppression pulse sequence.

Product Analysis. The gaseous phase products were analyzed on a Shimadzu GC-2014C gas chromatography system equipped with a flame ionization detector (FID) and a methanizer unit. The separation of CO, CH₄, and CO₂ was achieved via a TDX-01 packed column. The liquid oxygenates were quantified by ¹H NMR spectroscopy on an Avance 500 liquid NMR spectrometer (Bruker), using a water suppression pulse sequence (Watergate5). An external standard method was used to measure the concentration of each liquid product using a series of methanol solutions with known concentrations to establish a standard curve. Typically, an aliquot of the product solution (0.4 mL) and D₂O (0.1 mL) was mixed in a 5 mm NMR tube for measurement. The concentration of each liquid product was determined based on a standard curve.

RESULTS AND DISCUSSION

Methane Oxidation Using AuPd/ZSM-5 Catalysts. A series of AuPd/ZSM-5 (SiO₂/Al₂O₃ = 25) catalysts containing a total of 0.5 wt % metal were prepared with a range of Au: Pd ratios (Table S1 provides details of the ICP analysis) using the deposition precipitation method at pH 10 and with 2 h aging time. These catalysts were used for the oxidation of methane (Figure 1, Table S2) and it is apparent that the addition of Pd to Au/ZSM-5 increases the yield of acetic acid with the effect being most marked for the catalyst with the nominal loading of 0.375% Au + 0.125% Pd (analyzed concentrations of 0.34% Au + 0.115% Pd, Au: Pd molar ratio of 1.6, Table S1). For this catalyst, the C_{mol}-based ratio of C₂ products compared to C₁ products is enhanced to over 27 (Figure 1 and Table S2), approximately three times greater than that observed over the 0.5% Au/ZSM-5 analogue (C₂/C₁ = 9.3). The C₂/C₁ ratio was calculated on the basis of the moles of carbon atoms on the products. Therefore, the addition of Pd to Au/ZSM-5 markedly enhances the C₁ \rightarrow C₂ coupling step in the reaction. In addition, the catalysts did not show any leaching of the metals as a result of the methane oxidation reaction. In one experiment, we investigated the use of a physical mixture of 0.375 wt % Au/ZSM-5 and 0.125 wt % Pd/ZSM-5 and this did not show any enhancement in the C₂/C₁ ratio, which demonstrates that the Au and Pd must be in close contact to observe this effect.

The addition of Pd to Au was investigated using alternative supports (Table 1). Silica, alumina, zeolite Y, and mordenite also showed an enhancement of the C₂/C₁ ratio when Pd was added. However, the various H-ZSM-5 supports all showed a more

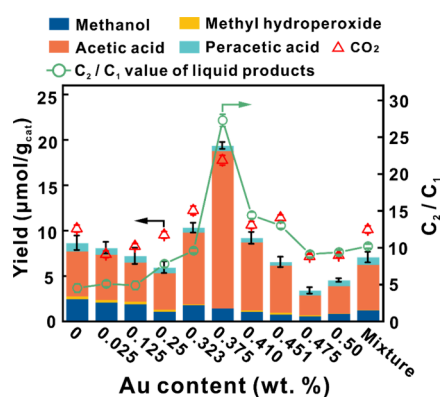


Figure 1. Product yield of methane oxidation on AuPd/ZSM-5 catalysts prepared with different Au and Pd metal loadings. The mixture was prepared by using 0.375 wt %Au/ZSM-5 (50 mg) and 0.125 wt % Pd/ZSM-5 (50 mg). Reaction conditions: catalyst (0.1 g), H₂O (15 mL), CH₄ (20.7 bar), O₂ (3.5 bar), 240 °C, 60 min, and 1000 rpm stirring.

marked enhancement in acetic acid formation with the effect increasing with an increasing SiO₂/Al₂O₃ ratio. Indeed, using silicalite-1, the alumina-free form of the MFI structure, showed the highest enhancement in the formation of acetic acid albeit at a reduced yield. These findings indicate that the acid site density of the support is not important for the effect on the C₂/C₁ ratio but it is helpful in enhancing liquid oxygenate yield.

We explored the effect of the reaction time over the 0.375% Au-0.125%Pd/ZSM-5 (SiO₂/Al₂O₃ = 25) catalyst (Figure 2a,c, Table S3), showing that the oxygenated products increase as expected with reaction time with CO₂ production rising steadily as well. Interestingly, the C₂/C₁ ratio is very high at the start but reaches a minimum after 2 h and then rises steadily. As the methane conversions in these experiments are low, the concentrations of methane and oxygen throughout this experiment will not change significantly. Hence, the changes we see in the product distribution, as denoted by the C₂/C₁ ratio, indicate that the catalyst structure is changing during the

course of the reaction. The underlying reason for this is discussed subsequently in this paper.

D₂O was used to explore the effect of solvent on the reaction. As shown in Figure 2b,d, methanol and CO₂ exhibited similar yields and trends with the reactions performed in H₂O. However, the acetic acid yield was significantly suppressed in the reactions in D₂O, resulting in a lower oxygenate yield and C₂/C₁ ratio in contrast to the reactions in H₂O.

These observations are consistent with our previous report³⁶ that methanol and acetic acid are formed from parallel C₁ oxidation and C–C coupling pathways through a network of surface-mediated processes. The C–C coupling pathway involves CH₃ surface bound radicals reacting with CO formed on the surface as methane is oxidized. The alternative fate of CO is to oxidize further to CO₂ and so we would expect that high C₂ yields will require a high CO population on the surface with an accompanied increase in CO₂. Indeed, plotting acetic acid yield against CO₂ yield shows the expected correlation both across the different Au:Pd ratios (Figure S1a) and for the time online using the optimal AuPd ratio with H₂O as solvent (Figure S1b). Interestingly, this correlation is lost when D₂O is used as solvent for which the acetic acid yield remains low even though the CO₂ yield increases with reaction time (Figure 2 and Figure S1b). The decreased yield likely results from the slower dissociation of acetic acid in D₂O compared with H₂O,⁴³ which impedes its desorption from the catalyst surface thereby reducing the overall product yield. This suggests that the solvent is involved in the formation of acetic acid but has little influence on the CO₂ yield (Table S3).

We investigated the effect of adding CO as a coreductant (Figure 3, Table S4) and it is clear that for Au/ZSM-5, the addition of CO enhances the formation of methanol as we have observed previously.³⁶ However, the effect is significantly less marked for catalysts containing Pd but the total yield of CO₂ is high.

Isotopic Labeling Experiments. The promoting effect of the Pd component on acetic acid production was studied by isotopic ¹³C tracing experiments (Table 2). In all these isotopic labeling studies, CO was a cofeed. For methane oxidation with the Au-only, Pd-only, and AuPd/ZSM-5 catalysts using 20%

Table 1. Methane Oxidation over 0.375%Au-0.125%Pd Catalysts Prepared by Using Different Supports^a

entry	catalyst	SiO ₂ /Al ₂ O ₃	yield (μmol/g _{cat})					oxygenate selectivity (%)	acetic acid selectivity in liquid (%)	C ₂ /C ₁ liquid products	oxygenate yield (μmol/g _{cat})
			methanol	methyl hydro peroxide	acetic acid	peracetic acid	CO ₂				
1	AuPd/SiO ₂		0.4	0	3.3	0.2	12.7	36.8	88.5	17.2	3.9
2	AuPd/Al ₂ O ₃		0.2	0	2.2	0	24.9	15.7	94.7	18.0	2.5
3	AuPd/ZSM-5	25	1.3	0	17.4	0.6	17.7	67.8	93.4	27.2	19.3
4	AuPd/ZSM-5	50	0.8	0	8.4	0	9.6	64.9	95.5	21.4	9.2
5	AuPd/ZSM-5	130	0.7	0	12.5	0	18.6	57.9	97.2	35.2	13.2
6	AuPd/ZSM-5	300	0.3	0	10.8	0	14.1	60.9	98.8	82.7	11.1
7	AuPd/Silicate-1	∞	0	0	2.5	0	16.3	23.2	100	∞	2.4
8	AuPd/H–Y	5	1.1	0.7	11.0	1.0	3.5	88.1	85.3	13.4	13.8
9	AuPd/H–MOR	20	1.3	0	11.8	0.6	10.7	70.8	90.4	19.7	13.7

^aReaction conditions: catalyst (0.1 g), H₂O (15 mL), CH₄ (20.7 bar), O₂ (3.5 bar), 240 °C, 60 min, and 1000 rpm stirring.

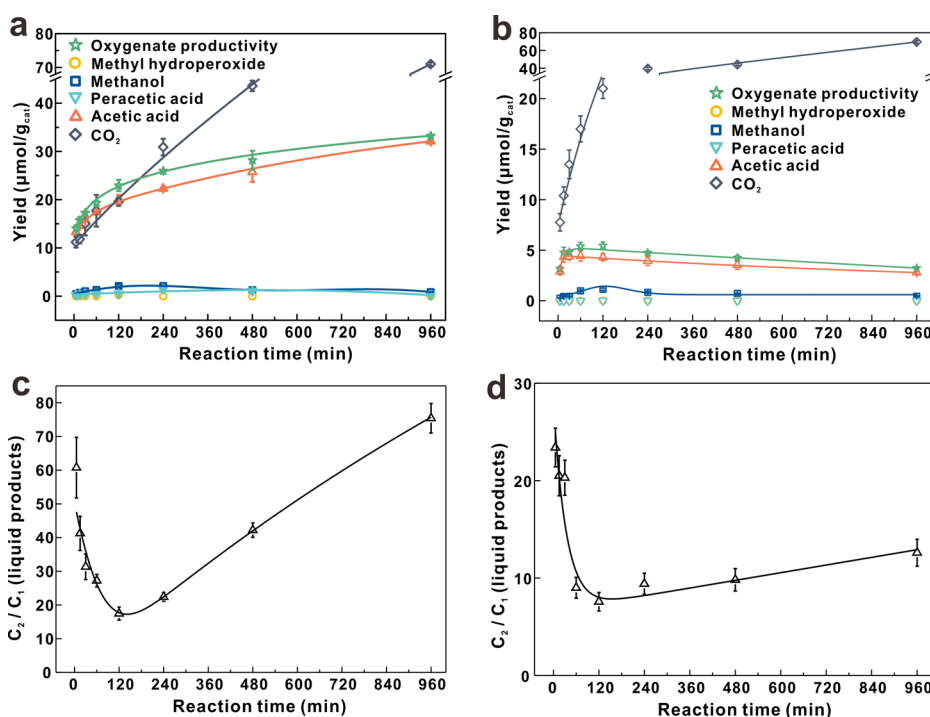


Figure 2. Time online analysis of the product yield (a, b) and C_2/C_1 ratio in the products (c, d) of methane oxidation over the 0.375%Au-0.125%Pd/ZSM-5 catalyst. Reaction conditions: catalyst (0.1 g), H_2O (a, c) or D_2O (b, d) (15 mL), CH_4 (20.7 bar), O_2 (3.5 bar), 240 °C, 1000 rpm stirring, and varying reaction times.

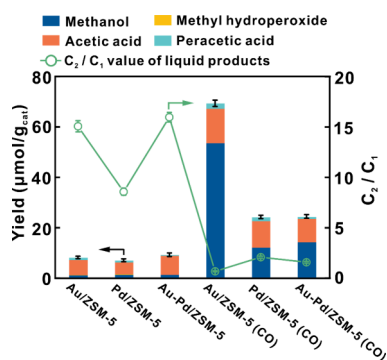


Figure 3. Comparison of product yield and C_2/C_1 ratio in the products of methane oxidation with or without CO on 0.375%Au-0.125%Pd/ZSM-5 catalysts. Reaction conditions: catalyst (0.1 g), H_2O (15 mL), CH_4 (20.7 bar), O_2 (2.5 bar), CO or N_2 (1.0 bar), 240 °C, 60 min, and 1000 rpm stirring.

^{13}C -enriched methane (Table 2, entry 1–3), it was clearly demonstrated that the ^{13}C label in the methane mainly contributes to the formation of methanol and the methyl group of acetic acid. Switching the ^{13}C -reagent to 20% ^{13}C -enriched CO caused the obvious increase of ^{13}C content on the carbonyl group of acetic acid on these catalysts (Table 2, entry 4–6). As predicted, the Pd-only and Au-only catalysts exhibited the highest (20.4%) and lowest (8.1%) ^{13}C content on the carbonyl group, respectively. Interestingly, AuPd/ZSM-5 showed a median ^{13}C content (18.4%) on the carbonyl group, much higher than that of the Au-only catalyst. These findings are consistent with the reaction mechanism we proposed in our initial study using the Au/ZSM-5 catalyst.³⁶

Catalyst Characterization. The fresh and used catalysts were examined using AC-STEM and EDS mapping (Figure 4 and Figures S2 and S3). Examination of the fresh catalysts

Table 2. ^{13}C Isotope Tracing Experiments for Methane Oxidation on Different Catalysts^{a,d}

entry	catalyst	^{13}C -enriched reagent	^{13}C abundance of products (%)		
			acetic acid		
			methanol	methyl	carbonyl
1 ^b	Au/ZSM-5	CH_4	10.7	6.5	2.1
2 ^b	Pd/ZSM-5		8.7	7.2	1.2
3 ^b	AuPd/ZSM-5		14.2	10.6	1.4
4 ^c	Au/ZSM-5	CO	1.2	2.3	8.1
5 ^c	Pd/ZSM-5		1.1	1.3	20.4
6 ^c	AuPd/ZSM-5		1.2	1.2	18.4

^aReaction conditions: Catalyst (0.1 g), H_2O (15 mL), CH_4 (20.7 bar), O_2 (2.5 bar), CO (1.0 bar), 240 °C, 60 min, and 1000 rpm stirring. ^b20% ^{13}C -enriched CH_4 was used. ^c20% ^{13}C -enriched CO was used. ^dThe Au loading for Au/ZSM-5 was 0.375 wt %, the Pd loading for Pd/ZSM-5 was 0.125 wt %, and the Au and Pd loadings for AuPd/ZSM-5 were 0.375 and 0.125 wt %, respectively.

showed it to comprise AuPd alloys with Au in excess, in agreement with the nominal Au:Pd ratio. Trace Fe was also found to be present (Figure 4a), and this is consistent with the low base concentration of Fe known to be present in ZSM-5.⁴⁴ ICPMS measurements conducted in the study confirm this. However, analysis of the catalyst used for 5 min (Figure 4 b) and 30 min (Figure 4 c) showed an increased concentration of Fe postreaction and the formation of an Fe shell on the Au–Pd nanoparticles. The extent of this Fe layer and its increase in concentration with longer reaction times could not be attributed to the migration of the initial low Fe present in the support nor to background Fe X-rays generated within the microscope from the column itself and hence are attributed to reactor leaching during the reaction.

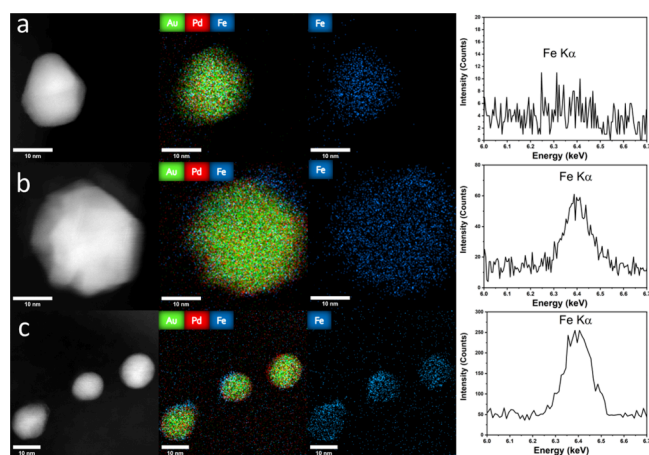


Figure 4. AC-HAADF-STEM images and EDS mapping analysis of AuPd/ZSM-5 catalysts with 0.375 wt % Au and 0.125 wt % Pd: fresh catalyst (a), used catalysts after 5 min (b), and used catalyst after 30 min (c). Energy-dispersive X-ray spectrum of the Fe region is also included for each catalyst. The spectrum is from the integrated counts over the entire view field shown. Reaction conditions: catalyst (0.1 g), H₂O (15 mL), CH₄ (20.7 bar), O₂ (3.5 bar), 240 °C, reaction time of 0–30 min.

Effect of Fe on the Oxidation of Methane Using AuPd/ZSM-5. The discovery that Fe from the autoclave reactor was deposited on the surface of the AuPd nanoparticles during the reaction prompted us to make a detailed study of the possible effects that Fe could have on observed catalysis. We initially investigated whether a glass liner in the same reactor could decrease the Fe deposition. As shown in Figure 5 and Table S5, acetic acid remains the dominant liquid product in the presence of the glass liner. However, the yield of acetic acid is decreased compared to reactions conducted without the liner, with this reduction increasing from ~8% at 60 min to ~32% at 960 min reaction time; this reduction is even more pronounced for the minor methanol yield. Additionally, the use of the glass liner results in a higher CO₂ yield. These observations suggest that overoxidation to CO₂ is more pronounced when using the glass liner, leading to reduced liquid oxygenate yield, particularly at longer reaction times. Inductively coupled plasma optical emission spectrometry (ICP-OES) was used to determine the Fe concentration on both fresh and used catalysts in the two reaction setups (Table 3). The fresh catalyst exhibits an Fe concentration of 460 ppm by weight, which increases to 2740 ppm after use in the reaction for 960 min without the glass liner.

Table 3. ICP Analysis of Fe Concentration on AuPd/ZSM-5 Catalysts with 0.375 wt % Au and 0.125 wt % Pd and Corresponding Supernatants^a

entry	sample	Fe concentration	
		(ppm)	(%) ^c
1	fresh AuPd/ZSM-5	460	
2	used AuPd/ZSM-5 (without glass liner)	1550 (2740) ^a	51
3	used AuPd/ZSM-5 (with glass liner)	780 (1410) ^a	72
4	used AuPd/ZSM-5 (without glass liner)	1240 ^b	20
5	supernatant (without glass liner)	10	49
6	supernatant (without glass liner)	40 ^b	80

^aData in parentheses show the results after 960 min of reaction. ^bThe catalyst-solution separation used hot filtration at 80 °C. All other entries used room-temperature filtration. ^cThe fraction of Fe on the catalyst is relative to the total Fe in both the supernatant and on the catalyst. ^dReaction conditions: catalyst (0.1 g), H₂O (15 mL), CH₄ (20.7 bar), O₂ (3.5 bar), 240 °C, reaction time of 60 min, and 1000 rpm stirring.

In contrast, the Fe concentration on the used catalyst after 960 min with the glass liner is 1410 ppm, significantly lower than that on the catalyst used without the glass liner. These results indicate that Fe species leached from the reactor can migrate onto the catalyst, affecting its performance in methane oxidation, consequently resulting in increased acetic acid production and reduced overoxidation. The observed Fe release under the reaction conditions can be attributed to incomplete coverage of the glass liner within the reactor, leaving exposed surfaces susceptible to corrosion. To investigate the migration of leached Fe onto the AuPd/ZSM-5 catalyst, samples filtered at room temperature (Table 3, entries 2 and 5) were compared with those filtered at 80 °C. Notably, the latter exhibits a marked difference, revealing a lower Fe concentration of 1240 ppm (wt) in the used catalyst and a higher Fe concentration of 40 ppm (wt) in the corresponding supernatant (Table 3, entries 4 and 6). This disparity suggests that the elevated temperature during filtration affects the distribution of iron species, influencing their deposition on the catalyst surface. Moreover, the significant increase in Fe concentration in the supernatant after hot filtration underscores the role of the temperature in altering the equilibrium between the solution and solid phases. The higher Fe content in the solution suggests that elevated temperatures enhance the dissolution of Fe species from the reactor or other surfaces, facilitating their transport into the reaction solution. However, the observation of the higher Fe concentration in

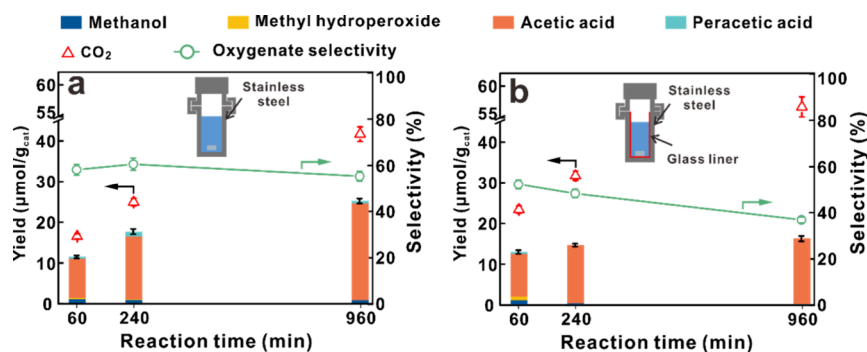


Figure 5. Methane oxidation over the AuPd/ZSM-5 catalyst with 0.375 wt % Au and 0.125 wt % Pd using the same reactor without (a) and with (b) a glass liner. Reaction conditions: catalyst (100 mg), H₂O (15 mL), CH₄ (20.7 bar), O₂ (3.5 bar), 240 °C, reaction time of 60–960 min, and 1000 rpm stirring.

solution with the hot filtration experiment can suggest that some of the Fe deposited on the catalyst may be the result of cooling the reactor.

The fresh AuPd/ZSM-5 catalyst exhibits a base Fe concentration of 460 ppm (wt), likely originating from the ZSM-5 support itself, which has a significantly higher Fe content of 950 ppm by weight (Table S6). This observation aligns with previous reports suggesting the presence of extra-framework metal species in zeolites (e.g., Fe).^{45–47} To minimize the influence of these Fe impurities, the ZSM-5 support was acid-treated with a 5 wt % HCl solution at 80 °C for 12 h. This treatment is known to effectively remove extra-framework metal species without altering the zeolite's framework structure,⁴⁸ as confirmed by XRD patterns and ²⁷Al and ²⁹Si MAS NMR spectra (Figure S4). Notably, the acid treatment successfully reduces the Fe concentration in the ZSM-5 support to 180 ppm (wt) (Table S6). Subsequently, we investigated the impact of these Fe species by performing methane oxidation reactions with AuPd/ZSM-5 catalysts in glass-lined reactors prepared by using both the original and acid-treated supports. This approach allows us to isolate and evaluate the role of Fe in the ZSM-5 support in methane oxidation activity.

As depicted in Figure 6 and Table S7, the yield of both liquid oxygenates and CO₂ is decreased for the AuPd/ZSM-5 catalyst

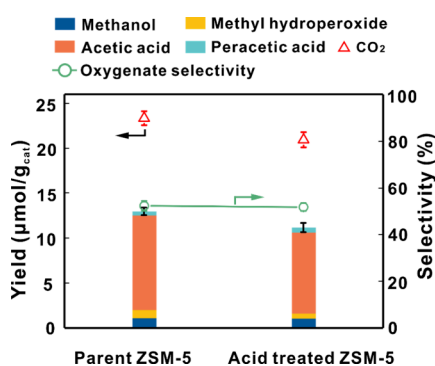


Figure 6. Methane oxidation on the AuPd/ZSM-5 catalyst with 0.375 wt % Au and 0.125 wt % Pd prepared with parent and acid-treated ZSM-5 support in a reactor with a glass liner. Reaction conditions: catalyst (0.1 g), H₂O (15 mL), CH₄ (20.7 bar), O₂ (3.5 bar), 240 °C, reaction time of 60 min, and 1000 rpm stirring.

prepared using the acid-treated support compared with the original catalyst. This suggests that the removal of Fe impurities

through acid treatment adversely affects the catalyst's performance. The reduced performance of the acid-treated catalyst highlights the promoting effect of Fe species in the support. Despite their potential to leach into the reaction mixture, these Fe species appear to enhance catalytic activity. This is consistent with previous studies suggesting that small amounts of Fe can act as cocatalysts or promoters in various oxidation reactions.^{49,50} The presence of Fe may influence the dispersion of the AuPd nanoparticles or create additional active sites on the catalyst surface. In controlled methane reactions with the ZSM-5 support, both untreated and acid-treated, it is evident that ZSM-5 supports without the AuPd species exhibit very low activity in methane oxidation (Table S8). This finding underscores that AuPd is the primary active phase in the catalytic process.

We have observed that Fe species, whether leached from the reactor or originating from the ZSM-5 support, can enhance methane oxidation over the AuPd/ZSM-5 catalyst. To elucidate the specific role by which Fe species influence the catalytic activity of the AuPd/ZSM-5 catalyst, we introduced various forms of Fe into the reaction medium. Specifically, Fe³⁺ (as Fe(NO₃)₃), metallic Fe (as iron powder), and Fe oxide (as Fe₂O₃) were added to the reaction liquid while using an AuPd/ZSM-5 catalyst prepared with an acid-treated support. All reactions were conducted in a reactor equipped with a glass liner to minimize any effects stemming from the reactor.

As depicted in Figure 7a,b and detailed in Table S9, the addition of varying amounts of Fe³⁺ or iron powder results in only slight changes in the yield of liquid oxygenates. This suggests that Fe³⁺ and iron powder exert a minimal influence on the catalytic activity of the AuPd/ZSM-5 catalyst. However, a different trend is observed with the addition of Fe₂O₃. The yield of liquid oxygenates and CO₂ follows a volcano pattern with varying amounts of Fe₂O₃ (Figure 7c), strongly indicating that added Fe₂O₃ plays an active role in enhancing the catalytic activity. The optimal performance was achieved with the addition of 1000 ppm Fe₂O₃, resulting in a maximum liquid oxygenate yield of 18.9 μmol/g_{cat}, predominantly acetic acid. This represents an increase of up to 42% compared to the reaction utilizing only the AuPd/ZSM-5 catalyst (Table S9). The addition of Fe₂O₃ significantly improves the catalyst's stability. As shown in Figure S5, the reaction without Fe₂O₃ exhibits a substantial decline in the product yield after three consecutive cycles. In contrast, the catalyst with added Fe₂O₃ maintains a stable and enhanced performance over the same period. The reaction using the postreaction supernatant shows that the homogeneous part contributes negligibly to the product

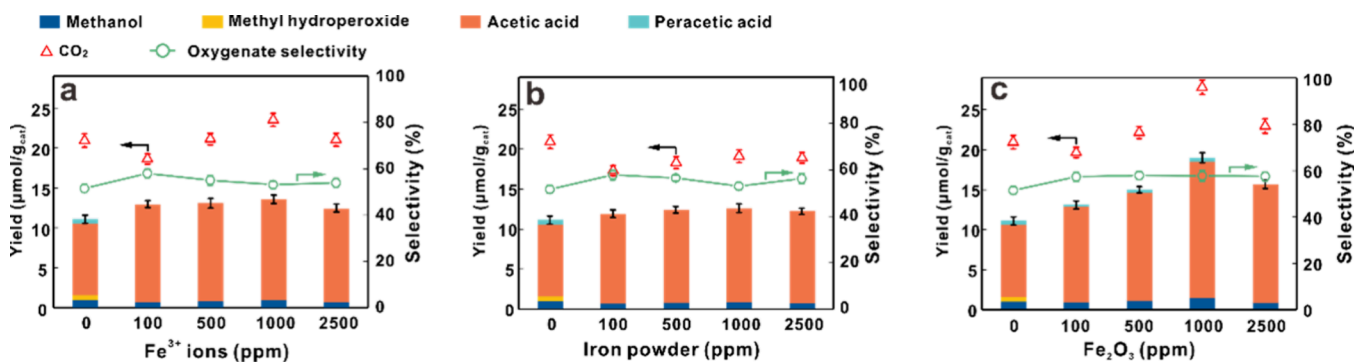


Figure 7. Methane oxidation over the AuPd/ZSM-5 catalyst with 0.375 wt % Au and 0.125 wt % Pd prepared using an acid-treated support with adding Fe³⁺ ions in a reactor with a glass liner (a), iron powder (b), and Fe₂O₃ (c) in the reaction medium. Reaction conditions: catalyst (0.1 g), different Fe sources (0–2500 ppm (wt)), H₂O (15 mL), CH₄ (20.7 bar), O₂ (3.5 bar), 240 °C, reaction time of 60 min, and 1000 rpm.

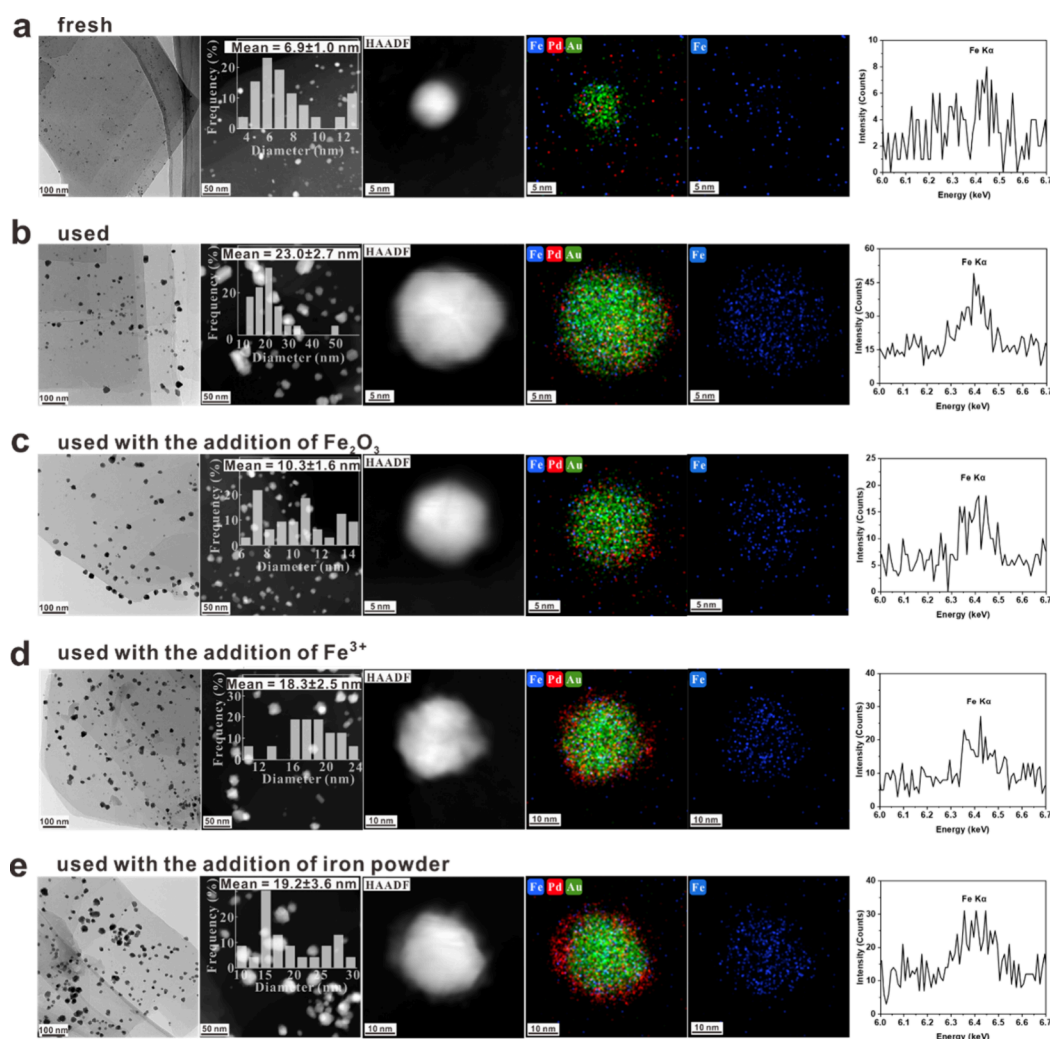


Figure 8. AC-HAADF-STEM images and EDS mapping analysis of AuPd/ZSM-5 catalysts with 0.375 wt % Au and 0.125 wt % Pd prepared using acid-treated support: fresh catalyst (a), used catalyst (b), used catalyst with 1000 ppm Fe_2O_3 addition (c), used catalyst with 1000 ppm Fe^{3+} addition (d), and used catalyst with 1000 ppm iron powder addition (e). Particle size distributions are also included for each catalyst. Energy-dispersive X-ray spectrum of the Fe region is also included for each catalyst. The spectrum is from the integrated counts over the entire view field shown. Reaction conditions: catalyst (0.1 g), H_2O (15 mL), CH_4 (20.7 bar), O_2 (3.5 bar), 240 °C, reaction time of 60 min, and 1000 rpm stirring in a reactor with a glass liner.

yield and selectivity (Figure S6). These findings highlight that the addition of Fe can affect the catalytic performance of the AuPd/ZSM-5 catalyst when added in very high amounts. It is possible that the different effects observed with the addition of Fe^0 , Fe^{3+} , and Fe_2O_3 are solely related to their relative solubility in these reaction conditions.

XPS analysis of the post-reaction Fe-treated samples reveals no signal in the Fe(2p) region for all samples tested (Figure S7), suggesting that the dispersion of the Fe is poor, if present at the surface, or its concentration is below the detection limits of the technique. Therefore, to elucidate the synergistic effect of added Fe_2O_3 with AuPd species on the AuPd/ZSM-5 catalyst during methane oxidation, aberration-corrected high-angle annular dark-field scanning transmission electron microscopy (AC-HAADF-STEM) and energy-dispersive X-ray spectroscopy (EDS) analyses were conducted to characterize the particle size and elemental distribution on the catalyst. As shown in Figure 8a, smooth nanoparticles with an average size of 7 nm were uniformly distributed on the fresh catalyst surface. EDS images confirmed that these nanoparticles were primarily

composed of Au, while Pd and Fe elements were uniformly dispersed across the zeolite support and the Fe was associated with the larger Au nanoparticles.

After 60 min of methane oxidation, the average nanoparticle size increased to 23 nm (Figure 8b). EDS images of the catalyst used revealed the presence of both Au and Pd within the nanoparticles, indicating agglomeration. The XPS spectra (Figure 9) of the fresh and used catalyst show no changes in binding energies, at least beyond that of the experimental uncertainty. For the fresh catalyst, the Pd content cannot readily be determined due to overlap with the Au $4d_{5/2}$ peak; however after use, the Pd 3d signal is clearly visible revealing both to Pd^0 and Pd^{2+} states.⁵¹ Interestingly, the addition of Fe_2O_3 does not affect the formation of the AuPd alloy but significantly inhibits nanoparticle agglomeration. The average nanoparticle size after 60 min of methane oxidation in the presence of Fe_2O_3 was 10 nm (Figure 8c), much smaller than that in its absence. EDS images also show an enhanced Fe signal, indicating a layer of Fe species coating the surface of the AuPd nanoparticles on the used catalyst. This oxidic Fe coating is particularly evident for the

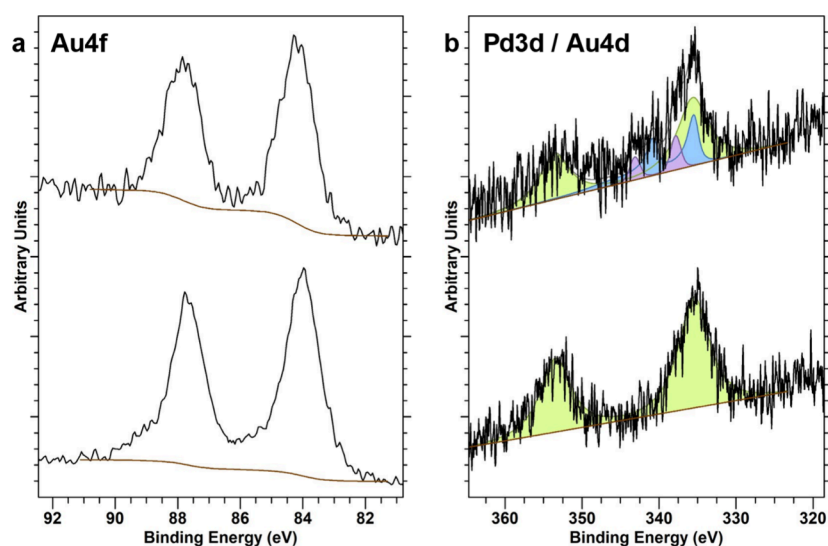


Figure 9. Au 4f (a) and Pd 3d/Au 4d (b) core-level spectra of the fresh (lower) and used (upper) AuPd/ZSM-5 catalyst with 0.375 wt % Au and 0.125 wt % Pd prepared with an acid-treated support. Reaction conditions: catalyst (0.1 g), H₂O (15 mL), CH₄ (20.7 bar), O₂ (3.5 bar), 240 °C, reaction time of 60 min, and 1000 rpm stirring in a reactor with a glass liner. Colors: green = Au⁰, blue = Pd⁰, and purple = Pd²⁺.

used samples following the addition of Fe₂O₃. The deposited oxidic Fe species may act as a secondary support for the AuPd nanoparticles, and these strong metal–support interactions are likely the driving force for the iron coating.^{52,53} It is possible that this oxidized Fe layer can play a role in stabilizing the nanoparticles and preventing excessive growth during the reaction.

The STEM and EDS analysis of the used catalyst with the addition of Fe³⁺ or iron powder reveals average particle sizes of the AuPd nanoparticles to be 18 and 19 nm, respectively (Figure 8d,e). This indicates that when iron is added as Fe³⁺ or Fe⁰, the iron is less effective in preventing active site agglomeration. The different effects observed with the addition of iron to the reaction mixture were considered to be related to the relative solubilities of the iron species under the reaction conditions.

CONCLUSIONS

In this study, we investigated the effect of the addition of Pd to the Au/ZSM-5 catalysts for the oxidation of methane in water at 240 °C with O₂ as the terminal oxidant. We observe that Pd addition can significantly enhance the formation of acetic acid. However, we also observe that under the aggressive reaction conditions, Fe can be leached from both the autoclave reactor and the ZSM-5. Consequently, we examined the impact of Fe on the activity and stability of AuPd/ZSM-5 in this liquid-phase reaction system. The leached Fe species are found to deposit on the AuPd/ZSM-5 catalyst during use and, when present in relatively high amounts, can promote methane oxidation and increase the yield of liquid oxygenates, primarily acetic acid. Control experiments, supported by STEM and EDS analyses, revealed that the Fe species leached from the reactor and ZSM-5 forms an oxidic iron coating on the AuPd nanoparticles during the reaction. This coating if sufficient can prevent the agglomeration of the AuPd nanoparticles, thereby enhancing the catalytic performance of the AuPd/ZSM-5 catalyst. These results provide valuable insights into the effects of reactor and catalyst corrosion on during methane oxidation under harsh reaction conditions, which have until now been largely not considered.

ASSOCIATED CONTENT

Supporting Information

The Supporting Information is available free of charge at <https://pubs.acs.org/doi/10.1021/acscatal.5c03918>.

Additional catalytic performance data and characterization data (PDF)

AUTHOR INFORMATION

Corresponding Authors

Jun Xu – National Centre for Magnetic Resonance in Wuhan, State Key Laboratory of Magnetic Resonance Spectroscopy and Imaging, Innovation Academy for Precision Measurement Science and Technology, Chinese Academy of Sciences, Wuhan 430071, China; University of Chinese Academy of Sciences, Beijing 100049, China; orcid.org/0000-0003-2741-381X; Email: xujun@wipm.ac.cn

Graham J. Hutchings – Max Planck Centre on the Fundamentals of Heterogeneous Catalysis, FUNCAT, Cardiff Catalysis Institute, School of Chemistry, Cardiff University, Translational Research Hub, Cardiff CF24 4HQ, United Kingdom; orcid.org/0000-0001-8885-1560; Email: Hutch@cardiff.ac.uk

Authors

Xu Li – National Centre for Magnetic Resonance in Wuhan, State Key Laboratory of Magnetic Resonance Spectroscopy and Imaging, Innovation Academy for Precision Measurement Science and Technology, Chinese Academy of Sciences, Wuhan 430071, China; University of Chinese Academy of Sciences, Beijing 100049, China

Guodong Qi – National Centre for Magnetic Resonance in Wuhan, State Key Laboratory of Magnetic Resonance Spectroscopy and Imaging, Innovation Academy for Precision Measurement Science and Technology, Chinese Academy of Sciences, Wuhan 430071, China; University of Chinese Academy of Sciences, Beijing 100049, China

Richard J. Lewis – Max Planck Centre on the Fundamentals of Heterogeneous Catalysis, FUNCAT, Cardiff Catalysis Institute, School of Chemistry, Cardiff University,

Translational Research Hub, Cardiff CF24 4HQ, United Kingdom; orcid.org/0000-0001-9990-7064

Mark J. Howard – Max Planck Centre on the Fundamentals of Heterogeneous Catalysis, FUNCAT, Cardiff Catalysis Institute, School of Chemistry, Cardiff University, Translational Research Hub, Cardiff CF24 4HQ, United Kingdom

Barry A. Murrer – Max Planck Centre on the Fundamentals of Heterogeneous Catalysis, FUNCAT, Cardiff Catalysis Institute, School of Chemistry, Cardiff University, Translational Research Hub, Cardiff CF24 4HQ, United Kingdom

Brian Harrison – Max Planck Centre on the Fundamentals of Heterogeneous Catalysis, FUNCAT, Cardiff Catalysis Institute, School of Chemistry, Cardiff University, Translational Research Hub, Cardiff CF24 4HQ, United Kingdom

David J. Morgan – Max Planck Centre on the Fundamentals of Heterogeneous Catalysis, FUNCAT, Cardiff Catalysis Institute, School of Chemistry, Cardiff University, Translational Research Hub, Cardiff CF24 4HQ, United Kingdom; orcid.org/0000-0002-6571-5731

Christopher J. Kiely – Department of Materials Science and Engineering, Lehigh University, Bethlehem, Pennsylvania PA 18015, United States

Qian He – National University of Singapore, Singapore 117575, Singapore

Thomas E. Davies – Max Planck Centre on the Fundamentals of Heterogeneous Catalysis, FUNCAT, Cardiff Catalysis Institute, School of Chemistry, Cardiff University, Translational Research Hub, Cardiff CF24 4HQ, United Kingdom

David J. Willock – Max Planck Centre on the Fundamentals of Heterogeneous Catalysis, FUNCAT, Cardiff Catalysis Institute, School of Chemistry, Cardiff University, Translational Research Hub, Cardiff CF24 4HQ, United Kingdom; orcid.org/0000-0002-8893-1090

Michael Bowker – Max Planck Centre on the Fundamentals of Heterogeneous Catalysis, FUNCAT, Cardiff Catalysis Institute, School of Chemistry, Cardiff University, Translational Research Hub, Cardiff CF24 4HQ, United Kingdom; orcid.org/0000-0001-5075-1089

Jingxian Cao – National Centre for Magnetic Resonance in Wuhan, State Key Laboratory of Magnetic Resonance Spectroscopy and Imaging, Innovation Academy for Precision Measurement Science and Technology, Chinese Academy of Sciences, Wuhan 430071, China; University of Chinese Academy of Sciences, Beijing 100049, China

Feng Deng – National Centre for Magnetic Resonance in Wuhan, State Key Laboratory of Magnetic Resonance Spectroscopy and Imaging, Innovation Academy for Precision Measurement Science and Technology, Chinese Academy of Sciences, Wuhan 430071, China; University of Chinese Academy of Sciences, Beijing 100049, China; orcid.org/0000-0002-6461-7152

Complete contact information is available at: <https://pubs.acs.org/10.1021/acscatal.5c03918>

Author Contributions

The manuscript was written through contributions of all authors. All authors have given approval to the final version of the manuscript.

Notes

The authors declare no competing financial interest.

ACKNOWLEDGMENTS

This work was supported by the National Key R&D Program of China (2022YFA1504500), the Strategic Priority Research Program of the Chinese Academy of Sciences (XDB0540000), the National Natural Science Foundation of China (22225205, 22272185, 22320102002, 22127801, 22161132028), the Youth Innovation Promotion Association of the Chinese Academy of Sciences (2021329), Hubei International Scientific and Technological Cooperation program (2024EHA043), and International Science & Technology Cooperation Base for Sustainable Catalysis and Magnetic Resonance (SH2303), the Young Top-Notch Talent Cultivation Program of Hubei Province, and the Sinopec Foundation (224250).

REFERENCES

- (1) International Energy Agency (IEA). *Global Methane Tracker 2024*; IEA: Paris, 2024. <https://www.iea.org/reports/global-methane-tracker-2024> (accessed 2025-5-25).
- (2) Dummer, N. F.; Willock, D. J.; He, Q.; Howard, M. J.; Lewis, R. J.; Qi, G.; Taylor, S. H.; Xu, J.; Bethell, D.; Kiely, C. J.; Hutchings, G. J. Methane Oxidation to Methanol. *Chem. Rev.* **2023**, *123*, 6359–6411.
- (3) Tang, P.; Zhu, Q.; Wu, Z.; Ma, D. Methane activation: the past and future. *Energy Environ. Sci.* **2014**, *7*, 2580–2591.
- (4) Choudhary, T. V.; Choudhary, V. R. Energy-Efficient Syngas Production through Catalytic Oxy-Methane Reforming Reactions. *Angew. Chem., Int. Ed.* **2008**, *47*, 1828–1847.
- (5) Wang, P.; Shi, R.; Zhao, Y.; Li, Z.; Zhao, J.; Zhao, J.; Waterhouse, G. I. N.; Wu, L.; Zhang, T. Selective Photocatalytic Oxidative Coupling of Methane via Regulating Methyl Intermediates over Metal/ZnO Nanoparticles. *Angew. Chem., Int. Ed.* **2023**, *62*, No. e202304301.
- (6) Gao, W.; Qi, G.; Wang, Q.; Wang, W.; Li, S.; Hung, I.; Gan, Z.; Xu, J.; Deng, F. Dual Active Sites on Molybdenum/ZSM-5 Catalyst for Methane Dehydroaromatization: Insights from Solid-State NMR Spectroscopy. *Angew. Chem., Int. Ed.* **2021**, *60*, 10709–10715.
- (7) Gao, W.; Wang, Q.; Qi, G.; Liang, J.; Wang, C.; Xu, J.; Deng, F. Active Ensembles in Methane Dehydroaromatization over Molybdenum/ZSM-5 Zeolite Identified by 2D 1H–95Mo Magic Angle Spinning Nuclear Magnetic Resonance Correlation Spectroscopy. *Angew. Chem., Int. Ed.* **2023**, *62*, No. e202306133.
- (8) Periana, R. A.; Taube, D. J.; Gamble, S.; Taube, H.; Satoh, T.; Fujii, H. Platinum Catalysts for the High-Yield Oxidation of Methane to a Methanol Derivative. *Science* **1998**, *280*, 560–564.
- (9) Periana, R. A.; Taube, D. J.; Evtitt, E. R.; Löffler, D. G.; Wentreck, P. R.; Voss, G.; Masuda, T. A Mercury-Catalyzed, High-Yield System for the Oxidation of Methane to Methanol. *Science* **1993**, *259*, 340–343.
- (10) Sen, A.; Benvenuto, M. A.; Lin, M.; Hutson, A. C.; Basickes, N. Activation of Methane and Ethane and Their Selective Oxidation to the Alcohols in Protic Media. *J. Am. Chem. Soc.* **1994**, *116*, 998–1003.
- (11) Jones, C. J.; Taube, D.; Ziatdinov, V. R.; Periana, R. A.; Nielsen, R. J.; Oxgaard, J.; Goddard, W. A. Selective Oxidation of Methane to Methanol Catalyzed, with C-H Activation, by Homogeneous, Cationic Gold. *Angew. Chem., Int. Ed.* **2004**, *43*, 4626–4629.
- (12) Banerjee, R.; Proshlyakov, Y.; Lipscomb, J. D.; Proshlyakov, D. A. Structure of the key species in the enzymatic oxidation of methane to methanol. *Nature* **2015**, *518*, 431–434.
- (13) Rosenzweig, A. C.; Frederick, C. A.; Lippard, S. J.; Nordlund, P. Crystal structure of a bacterial non-haem iron hydroxylase that catalyses the biological oxidation of methane. *Nature* **1993**, *366*, 537–543.
- (14) Lieberman, R. L.; Rosenzweig, A. C. Crystal structure of a membrane-bound metalloenzyme that catalyses the biological oxidation of methane. *Nature* **2005**, *434*, 177–182.

- (15) Balasubramanian, R.; Smith, S. M.; Rawat, S.; Yatsunyk, L. A.; Stemmler, T. L.; Rosenzweig, A. C. Oxidation of methane by a biological dicopper centre. *Nature* **2010**, *465*, 115–119.
- (16) Snyder, B. E. R.; Vanelderren, P.; Bols, M. L.; Hallaert, S. D.; Böttger, L. H.; Ungur, L.; Pierloot, K.; Schoonheydt, R. A.; Sels, B. F.; Solomon, E. I. The active site of low-temperature methane hydroxylation in iron-containing zeolites. *Nature* **2016**, *536*, 317–327.
- (17) Wood, B. R.; Reimer, J. A.; Bell, A. T.; Janicke, M. T.; Ott, K. C. Methanol formation on Fe/Al-MFI via the oxidation of methane by nitrous oxide. *J. Catal.* **2004**, *225*, 300–306.
- (18) Sobolev, V. I.; Dubkov, K. A.; Panna, O. V.; Panov, G. I. Selective oxidation of methane to methanol on a FeZSM-5 surface. *Catal. Today* **1995**, *24*, 251–252.
- (19) Woertink, J. S.; Smeets, P. J.; Groothaert, M. H.; Vance, M. A.; Sels, B. F.; Schoonheydt, R. A.; Solomon, E. I. A $[\text{Cu}_2\text{O}]^{2+}$ core in Cu-ZSM-5, the active site in the oxidation of methane to methanol. *Proc. Natl. Acad. Sci. U.S.A.* **2009**, *106*, 18908–18913.
- (20) Groothaert, M. H.; Smeets, P. J.; Sels, B. F.; Jacobs, P. A.; Schoonheydt, R. A. Selective Oxidation of Methane by the Bis(μ -oxo)dicopper Core Stabilized on ZSM-5 and Mordenite Zeolites. *J. Am. Chem. Soc.* **2005**, *127*, 1394–1395.
- (21) Narsimhan, K.; Michaelis, V. K.; Mathies, G.; Gunther, W. R.; Griffin, R. G.; Román-Leshkov, Y. Methane to Acetic Acid over Cu-Exchanged Zeolites: Mechanistic Insights from a Site-Specific Carbonylation Reaction. *J. Am. Chem. Soc.* **2015**, *137*, 1825–1832.
- (22) Sushkevich, V. L.; Palagin, D.; Ranocchiaro, M.; van Bokhoven, J. A. Selective anaerobic oxidation of methane enables direct synthesis of methanol. *Science* **2017**, *356*, 523–527.
- (23) Dinh, K. T.; Sullivan, M. M.; Narsimhan, K.; Serna, P.; Meyer, R. J.; Dincă, M.; Román-Leshkov, Y. Continuous Partial Oxidation of Methane to Methanol Catalyzed by Diffusion-Paired Copper Dimers in Copper-Exchanged Zeolites. *J. Am. Chem. Soc.* **2019**, *141*, 11641–11650.
- (24) Narsimhan, K.; Iyoki, K.; Dinh, K.; Román-Leshkov, Y. Catalytic Oxidation of Methane into Methanol over Copper-Exchanged Zeolites with Oxygen at Low Temperature. *ACS Cent. Sci.* **2016**, *2*, 424–429.
- (25) Cui, X.; Li, H.; Wang, Y.; Hu, Y.; Hua, L.; Li, H.; Han, X.; Liu, Q.; Yang, F.; He, L.; Chen, X.; Li, Q.; Xiao, J.; Deng, D.; Bao, X. Room-Temperature Methane Conversion by Graphene-Confined Single Iron Atoms. *Chem.* **2018**, *4*, 1902–1910.
- (26) Zhu, K.; Liang, S.; Cui, X.; Huang, R.; Wan, N.; Hua, L.; Li, H.; Chen, H.; Zhao, Z.; Hou, G.; Li, M.; Jiang, Q.; Yu, L.; Deng, D. Highly efficient conversion of methane to formic acid under mild conditions at ZSM-5-confined Fe-sites. *Nano Energy* **2021**, *82*, No. 105718.
- (27) Cheng, Q.; Li, G.; Yao, X.; Zheng, L.; Wang, J.; Emwas, A.-H.; Castaño, P.; Ruiz-Martínez, J.; Han, Y. Maximizing Active Fe Species in ZSM-5 Zeolite Using Organic-Template-Free Synthesis for Efficient Selective Methane Oxidation. *J. Am. Chem. Soc.* **2023**, *145*, 5888–5898.
- (28) Wu, B.; Lin, T.; Lu, Z.; Yu, X.; Huang, M.; Yang, R.; Wang, C.; Tian, C.; Li, J.; Sun, Y.; Zhong, L. Fe binuclear sites convert methane to acetic acid with ultrahigh selectivity. *Chem.* **2022**, *8*, 1658–1672.
- (29) Agarwal, N.; Freakley, S. J.; McVicker, R. U.; Althabhan, S. M.; Dimitratos, N.; He, Q.; Morgan, D. J.; Jenkins, R. L.; Willock, D. J.; Taylor, S. H.; Kiely, C. J.; Hutchings, G. J. Aqueous Au-Pd colloids catalyze selective CH_4 oxidation to CH_3OH with O_2 under mild conditions. *Science* **2017**, *358*, 223–227.
- (30) Ab Rahim, M. H.; Forde, M. M.; Jenkins, R. L.; Hammond, C.; He, Q.; Dimitratos, N.; Lopez-Sanchez, J. A.; Carley, A. F.; Taylor, S. H.; Willock, D. J.; Murphy, D. M.; Kiely, C. J.; Hutchings, G. J. Oxidation of Methane to Methanol with Hydrogen Peroxide Using Supported Gold–Palladium Alloy Nanoparticles. *Angew. Chem., Int. Ed.* **2013**, *52*, 1280–1284.
- (31) Jin, Z.; Wang, L.; Zuidema, E.; Mondal, K.; Zhang, M.; Zhang, J.; Wang, C.; Meng, X.; Yang, H.; Mesters, C.; Xiao, F.-S. Hydrophobic zeolite modification for in situ peroxide formation in methane oxidation to methanol. *Science* **2020**, *367*, 193–197.
- (32) Shan, J.; Li, M.; Allard, L. F.; Lee, S.; Flytzani-Stephanopoulos, M. Mild oxidation of methane to methanol or acetic acid on supported isolated rhodium catalysts. *Nature* **2017**, *551*, 605–609.
- (33) Tang, Y.; Li, Y.; Fung, V.; Jiang, D. e.; Huang, W.; Zhang, S.; Iwasawa, Y.; Sakata, T.; Nguyen, L.; Zhang, X.; Frenkel, A. I.; Tao, F. Single rhodium atoms anchored in micropores for efficient transformation of methane under mild conditions. *Nat. Commun.* **2018**, *9*, 1231.
- (34) Wang, S.; Fung, V.; Hülsey, M. J.; Liang, X.; Yu, Z.; Chang, J.; Folli, A.; Lewis, R. J.; Hutchings, G. J.; He, Q.; Yan, N. H_2 -reduced phosphomolybdate promotes room-temperature aerobic oxidation of methane to methanol. *Nat. Catal.* **2023**, *6*, 895–905.
- (35) Mao, J.; Liu, H.; Cui, X.; Zhang, Y.; Meng, X.; Zheng, Y.; Chen, M.; Pan, Y.; Zhao, Z.; Hou, G.; Hu, J.; Li, Y.; Xu, G.; Huang, R.; Yu, L.; Deng, D. Direct conversion of methane with O_2 at room temperature over edge-rich MoS_2 . *Nat. Catal.* **2023**, *6*, 1052–1061.
- (36) Qi, G.; Davies, T. E.; Nasrallah, A.; Sainna, M. A.; Howe, A. G. R.; Lewis, R. J.; Quesne, M.; Catlow, C. R. A.; Willock, D. J.; He, Q.; Bethell, D.; Howard, M. J.; Murrer, B. A.; Harrison, B.; Kiely, C. J.; Zhao, X.; Deng, F.; Xu, J.; Hutchings, G. J. Au-ZSM-5 catalyses the selective oxidation of CH_4 to CH_3OH and CH_3COOH using O_2 . *Nat. Catal.* **2022**, *5*, 45–54.
- (37) Cao, J.; Qi, G.; Yao, B.; He, Q.; Lewis, R. J.; Li, X.; Deng, F.; Xu, J.; Hutchings, G. J. Partially Bonded Aluminum Site on the External Surface of Post-treated Au/ZSM-5 Enhances Methane Oxidation to Oxygenates. *ACS Catal.* **2024**, *14*, 1797–1807.
- (38) Cao, J.; Lewis, R. J.; Qi, G.; Bethell, D.; Howard, M. J.; Harrison, B.; Yao, B.; He, Q.; Morgan, D. J.; Ni, F.; Sharma, P.; Kiely, C. J.; Li, X.; Deng, F.; Xu, J.; Hutchings, G. J. Methane Conversion to Methanol Using Au/ZSM-5 is Promoted by Carbon. *ACS Catal.* **2023**, *13*, 7199–7209.
- (39) Qi, G.; Davies, T. E.; Nasrallah, A.; Sainna, M. A.; Howe, A. G. R.; Lewis, R. J.; Quesne, M.; Catlow, C. R. A.; Willock, D. J.; Yao, B.; He, Q.; Bethell, D.; Howard, M. J.; Murrer, B. A.; Harrison, B.; Kiely, C. J.; Zhao, X.; Deng, F.; Xu, J.; Hutchings, G. J. Addendum: Au-ZSM-5 catalyses the selective oxidation of CH_4 to CH_3OH and CH_3COOH using O_2 . *Nat. Catal.* **2025**, *8*, 749–751.
- (40) Enache, D. I.; Edwards, J. K.; Landon, P.; Solsona-Espriu, B.; Carley, A. F.; Herzing, A. A.; Watanabe, M.; Kiely, C. J.; Knight, D. W.; Hutchings, G. J. Solvent-Free Oxidation of Primary Alcohols to Aldehydes Using Au-Pd/TiO₂ Catalysts. *Science* **2006**, *311*, 362–365.
- (41) Cooper, C. M.; Wiezevich, P. J. Effects of Temperature and Pressure on the Upper Explosive Limit of Methane-Oxygen Mixtures. *Ind. Eng. Chem.* **1929**, *21*, 1210–1214.
- (42) Morgan, D. J. The Utility of Adventitious Carbon for Charge Correction: A Perspective From a Second Multiuser Facility. *Surf. Interface Anal.* **2025**, *57*, 28–35.
- (43) Bunton, C. A.; Shiner, V. J., Jr. Isotope Effects in Deuterium Oxide Solution. I. Acid-Base Equilibria. *J. Am. Chem. Soc.* **1961**, *83*, 42–47.
- (44) Pirutko, L. V.; Chernyavsky, V. S.; Uriarte, A. K.; Panov, G. I. Oxidation of benzene to phenol by nitrous oxide: Activity of iron in zeolite matrices of various composition. *Appl. Catal. A: Gen.* **2002**, *227*, 143–157.
- (45) Hammond, C.; Dimitratos, N.; Jenkins, R. L.; Lopez-Sanchez, J. A.; Kondrat, S. A.; Hasbi ab Rahim, M.; Forde, M. M.; Thetford, A.; Taylor, S. H.; Hagen, H.; Stangland, E. E.; Kang, J. H.; Moulijn, J. M.; Willock, D. J.; Hutchings, G. J. Elucidation and Evolution of the Active Component within Cu/Fe/ZSM-5 for Catalytic Methane Oxidation: From Synthesis to Catalysis. *ACS Catal.* **2013**, *3*, 689–699.
- (46) Shahami, M.; Shantz, D. F. Zeolite acidity strongly influences hydrogen peroxide activation and oxygenate selectivity in the partial oxidation of methane over M, Fe-MFI (M: Ga, Al, B) zeolites. *Cata. Sci. Technol.* **2019**, *9*, 2945–2951.
- (47) Taran, O. P.; Yashnik, S. A.; Boltenev, V. V.; Parkhomchuk, E. V.; Sashkina, K. A.; Ayusheev, A. B.; Babushkin, D. E.; Parmon, V. N. Formic Acid Production Via Methane Peroxide Oxidation Over Oxalic Acid Activated Fe-MFI Catalysts. *Top. Catal.* **2019**, *62*, 491–507.
- (48) Richards, N.; Nowicka, E.; Carter, J. H.; Morgan, D. J.; Dummer, N. F.; Golunski, S.; Hutchings, G. J. Investigating the Influence of Fe Speciation on N_2O Decomposition Over Fe-ZSM-5 Catalysts. *Top. Catal.* **2018**, *61*, 1983–1992.

(49) Lipiec, W.; Sobczak, J. M.; Trzeciak, A. M. The influence of rotational motion of Fe and Fe/Cu nanowires on their activity when applied as co-catalysts in aerobic oxidation of acrolein catalyzed by N-hydroxyphthalimide. *Appl. Catal. A: Gen.* **2015**, *506*, 8–13.

(50) Schubert, J. S.; Popovic, J.; Haselmann, G. M.; Nandan, S. P.; Wang, J.; Giesriegel, A.; Cherevan, A. S.; Eder, D. Immobilization of Co, Mn, Ni and Fe oxide co-catalysts on TiO₂ for photocatalytic water splitting reactions. *J. Mater. Chem. A* **2019**, *7*, 18568–18579.

(51) Bukhtiyarov, A. V.; Prosvirin, I. P.; Bukhtiyarov, V. I. XPS/STM study of model bimetallic Pd–Au/HOPG catalysts. *Appl. Surf. Sci.* **2016**, *367*, 214–221.

(52) van Deelen, T. W.; Hernández Mejía, C.; de Jong, K. P. Control of metal-support interactions in heterogeneous catalysts to enhance activity and selectivity. *Nat. Catal.* **2019**, *2*, 955–970.

(53) Qiao, B.; Liang, J.-X.; Wang, A.; Xu, C.-Q.; Li, J.; Zhang, T.; Liu, J. J. Ultrastable single-atom gold catalysts with strong covalent metal-support interaction (CMSI). *Nano Res.* **2015**, *8*, 2913–2924.



CAS INSIGHTS™

EXPLORE THE INNOVATIONS SHAPING TOMORROW

Discover the latest scientific research and trends with CAS Insights. Subscribe for email updates on new articles, reports, and webinars at the intersection of science and innovation.

Subscribe today

CAS
A Division of the
American Chemical Society